Proceedings of ESAV'08 - September 3 - 5 - Capri, Italy

Passive emitter location with Doppler frequency and interferometric measurements

J.S. Groot, F.A.M. Dam, and A. Theil
TNO Defence, Security and Safety
Oude Waalsdorperweg 63, 2597 AK, The Hague, The Netherlands
phone: + (31) 70 3740432, fax: + (31) 70 3740654, email: jos.groot@tno.nl

***Abstract*— Ground based emitters can be located with a receiver installed on an airborne platform. This paper discusses techniques based on Doppler frequency and differential phase measurements (interferometry). Measurements of the first technique are provided, while we discuss and compare the theoretical accuracy of both. In addition, we demonstrate the use of simulated annealing for finding flight tracks that lead to the smallest location error.**

***Index Terms*— emitter location, Doppler frequency, interferometry, track optimization**

I. Introduction

Ground based emitters (like radar systems) transmit signals that can be used to estimate the emitter position from an aircraft. For example, a time series of Doppler frequencies (modulated on the emitter frequency) and/or phase measurements (interferometry) can be used. This is discussed for Doppler measurements in [1] and [4]. The latter article compares also Doppler and interferometric measurements. Both articles deal with simulated data only. We conducted an experiment in which Doppler data was acquired of air traffic control radars. The particulars and location accuracy results are given in Section II, in conjunction with an analysis of the sensitivity of the accuracy to some parameters. This sensitivity information can be used to adjust the flight track of the measuring platform so as to achieve a better accuracy. Section III repeats the sensitivity analysis for the interferometric case. Section IV demonstrates the benefit of combining Doppler and interferometric measurements. An interesting problem is that of finding the flight track that leads to the best location accuracy. A solution is for example provided in [6]. We use simulated annealing and show that this flexible Monte Carlo method provides almost identical results (Section V). Finally, in Section VI two software tools we developed and used for this research are considered.

II. Location with Doppler Frequencies

A. Theory

Due to aircraft movement, the radio frequency (RF) received on board from a ground based emitter contains a Doppler frequency shift. This component depends on the emitter location, amongst other. By combining it with aircraft position and velocity measurements one can estimate the emitter location. The basic algorithm is outlined in Figure 1.

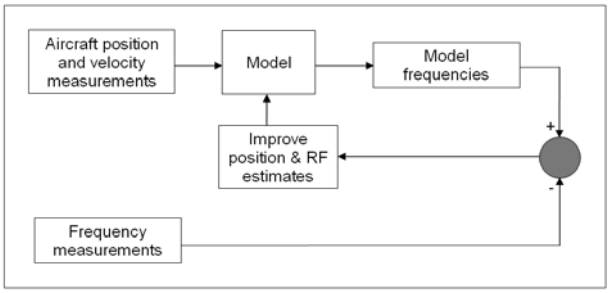

Figure 1 - Flow diagram for the basic Doppler based emitter location algorithm.

The algorithm calculates the model frequencies from the current estimate of the emitter location and the aircraft position and velocity with the $f(t,\mathbf{x})$ term of the measurement equation

$$\tilde{f}(t) = f(t,\mathbf{x}) + \nu(t) = f_0 - \frac{f_0}{c} v\hat{\mathbf{v}}(t)\cdot\hat{\mathbf{u}}(t) + \nu(t)\,. \qquad (1)$$

$\mathbf{x}$ is the four dimensional vector (x_e y_e z_e f_0) which consists of the RF and 3D location. The measured frequency $\tilde{f}(t)$ is the emitter frequency minus a small term, the Doppler frequency shift, plus measurement noise $\nu(t)$. The Doppler shift depends on the line-of-sight component of the aircraft velocity, which is the aircraft speed v times the vector dot-product of the aircraft unit velocity $\hat{\mathbf{v}}(t)$ and $\hat{\mathbf{u}}(t)$, the unit vector pointing from the emitter to the receiver. The algorithm minimizes the least squares sum S

$$S = \sum_{i=1}^{N}\left[\tilde{f}(t_i) - f(t_i,\mathbf{x})\right]^2 \qquad (2)$$

to find the optimum vector $\mathbf{x}$. This non-linear four-parameter minimization problem is solved with the standard iterative Gauss-Newton method [1, 3].

B. Measurements

We performed measurement flights sampling several air traffic control radars. These radars transmits at four slightly different RFs near 2.8 GHz. The chirped waveform complicates

This work was sponsored by the Netherlands Ministry of Defence under the EW research program V408.

consistent pulse-to-pulse frequency estimation. However, the chirp is mirror symmetric around a certain time t_0:

$$f(t_0 - \Delta t) + f(t_0 + \Delta t) = 2 f_0 . \quad (3)$$

We utilized this symmetry by estimating the central frequency f_0 at t_0, separately for each of the four RFs [2]. Figure 2 compares measured (averaged over the four RFs) and calculated Doppler frequencies as a function of time for a particular measurement. The large variation in Doppler frequency indicates that the aircraft was manoeuvring considerably. Along the track the aircraft-emitter distance varied from 55 to 77 km, with the aircraft speed being near 90 m/s.

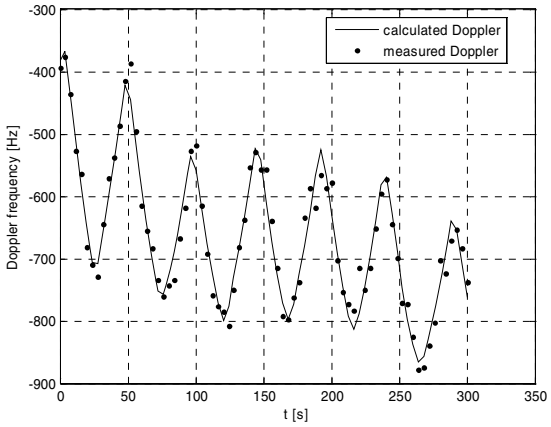

Figure 2 – Measured and calculated Doppler frequencies. The standard deviation of the difference is 19 Hz.

The calculated Doppler frequencies stem from the model, with the emitter location and RF being the least squares solution. We extended the basic four parameter algorithm to incorporate the additional RFs. We combined all possible combinations of the four frequencies (i.e., 1, 2, 3 or 4 frequencies) and found that the use of more frequencies does not always lead to a higher accuracy. The location error is on average about 2.2 km, which amounts to a relative error of ~ 3 %. The largest contribution to this error is due to the frequency error caused by the complicated (chirped) waveform. Another factor is the rather low aircraft speed.

C. *Additional findings from simulations*

The minimum least squares algorithm estimates four parameters. This can be reduced to two. The estimation of RF f_0 can be eliminated by minimizing the sum

$$S' = \sum_{i=1}^{N} \left[\tilde{f}(t_i) - f(t_i, f_0', \mathbf{x}') - m \right]^2 , \quad (4)$$

instead of the sum of Eq.(2), with

$$m = \bar{\tilde{f}} - \bar{f}(f_0', \mathbf{x}') . \quad (5)$$

Subtraction of the time average m removes a constant offset in the bracketed term of Eq.(4). Instead of fitting the RF f_0, we use a (fixed) measured RF f_0', which gives an error of at most the maximum Doppler frequency + measurement noise. It can be shown that the estimated location is quite insensitive to f_0', which legitimates the use of a measured value. The algorithm is also fairly insensitive to the emitter height. Using zero height for the emitter is therefore valid for our test area (The Netherlands). This reduces the basic four parameter algorithm to a two parameter one: only the 2D position $\mathbf{x}' = (x\ y)^T$ is estimated. However, the dimensionality of the algorithm does not clearly influence the accuracy or stability.
We also investigated the influence of the measurement time on the location error. On average, the error decreases with larger measurement time, but large excursions to small and large errors occur. This is at least partially due to the measurement noise, which gives different errors for different realizations.

D. *Accuracy*

It is possible to derive relations between measurement errors and system parameters, and location errors. We will use the basic algorithm that estimates four parameters (location + RF) but will restrict ourselves to the errors in the x- and y-coordinates of the location. The Cramér-Rao Lower Bound (CRLB) for these errors is derived in Appendix A. It also shows how to derive an expression for the dependence of the location error on the RF (measurement) error. The following table summarizes the dependence of the location error (x- and y-coordinates) on four more quantities for which analytical relations could be derived. The results are also valid for the z-error because the z-direction is not fundamentally different from the other two.

quantity	**location error dependence**
frequency error σ_f	σ_f
aircraft velocity error σ_v	σ_v
aircraft position error σ_p	σ_p
RF f_0	$1/f_0$
time interval dt	$\sqrt{dt}$ (dt< 1 s)

Table 1 – Linear dependencies of location errors for Doppler location.

Note the difference between the top three quantities, which are errors, and the lower two, which are not. For example, the location error is linearly proportional to an error in the measured velocity itself, and inversely proportional to the RF. Errors in the right column can be combined by taking the RMS value.

III. INTERFEROMETRIC LOCATION

Interferometric emitter location uses two separated antennas mounted on an airborne platform, in order to estimate the location of a ground based emitter. The setup is given in Figure 3. The antennas separated by the baseline length d receive the signal of the emitter, and the phase difference is used in the location procedure.

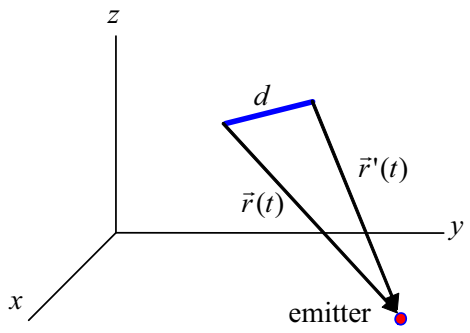

Figure 3 – Measurement geometry.

The measured phase difference [rad] between the primary and secondary antenna is

$$\tilde{\alpha}(t) = \frac{2\pi}{\lambda}\left(|\mathbf{r}(t)| - |\mathbf{r}'(t)|\right) + \delta\alpha(t), \quad (6)$$

with

λ emitter wavelength [m]
$\mathbf{r}$ vector from the primary antenna to the emitter [m]
$\mathbf{r}'$ ditto for the secondary antenna (closest to the front of the aircraft) [m].
$\delta\alpha$ phase measurement noise [rad]

Because the baseline is small compared to the emitter distance, a good approximation for this equation is

$$\tilde{\alpha}(t) = \frac{2\pi d}{\lambda}\sin\beta(t) + \delta\alpha(t), \quad (7)$$

with β the angle between the perpendicular to the baseline and the Line Of Sight (LOS). This equation shows that for baselines $d < \lambda/2$ the phase is always contained in the interval $[-\pi, \pi]$ (neglecting noise), i.e., no wraparound occurs. This is the condition for Short Baseline Interferometry (SBI). In Long Baseline Interferometry (LBI) $d \geq \lambda/2$ and wraparound can occur, and measures should be taken to enable recovery of the unwrapped phase. In the same manner as for the previous Doppler case we can derive relations for the estimation errors for SBI, see Table 2.

quantity	**location error dependence**
phase error $\delta\alpha$	$\delta\alpha$
aircraft attitude errors σ_θ σ_φ	$\max(\sigma_\theta, \sigma_\varphi)$
baseline length d	$1/d$
wavelength λ	λ
time interval dt	$\sqrt{dt}$ ($dt < 1$ s)

Table 2 – Linear dependencies of location errors for SBI.

We assumed in the above that the baseline is parallel to the fuselage. For LBI these relations hold at most approximately. Some of the dependencies can be derived by noting similarities between Eq.(1) and Eq.(7), if the latter is rewritten as

$$\tilde{\alpha}(t) = \frac{2\pi f_0}{c} d\hat{\mathbf{d}}(t)\cdot\hat{\mathbf{u}}(t) + \delta\alpha(t), \quad (8)$$

with $\hat{\mathbf{d}}$ and $\hat{\mathbf{u}}$ unit vectors in the baseline and LOS directions, respectively. For example, because f_0 (~ $1/\lambda$) occurs in the same role in Eq.(1) and (7) the dependency is the same. The relations of Tables 1-2 were confirmed by numerical simulations. Those of Table 2 also agree with the specific analytical solution for the straight track example of [4].

IV. Combining Doppler and Interferometric Location

Appendix B shows that combining (different) measurements always increases the accuracy. This is an example of low level fusion, i.e., combining Doppler and phase measurements directly. We compare this with high level fusion (averaging position estimates) for the combined Doppler and interferometric technique in Figure 4.

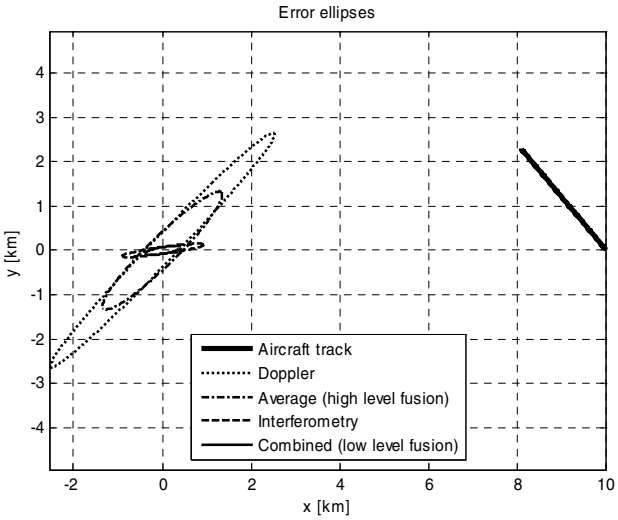

Figure 4 – Low and high level fusion compared. The ellipse area decreases from top to bottom in the legend (Doppler, ..., Combined).

The line segment at the right is the aircraft track. It is clear that low level fusion performs better than high level fusion. In the former case the error ellipse is entirely inside those of the separate techniques. This is not true for the high level ellipse.

V. Track Optimization

Finding the flight track providing the smallest location error in a fixed amount of time has been the subject of previous research [6]. We used Simulated Annealing (SA) [3] to solve this problem. This is a method to solve high dimensional problems *approximately*. The method borrows its name from a

method ('annealing') for cooling a liquid slowly (if a liquid is cooled down slowly it crystallizes. This ordered final state has (almost) minimal energy. This minimization process is mimicked by SA). We start with a certain non-optimal track consisting of straight segments. The track, parameterized by the segment angles and a constant segment length, is than varied to find a (local) minimum. In doing this, it is allowed (with a certain probability *P*) to (temporarily) become even more non-optimum. In this way it circumvents sticking to a bad local minimum. The probability *P* decreases with time. So a sequence of (on average) decreasing local minima is visited. Mostly, the global minimum is not found. However, many high dimensional minimization problems exhibit many local minima which are almost as deep as the global one. SA will than often find such a near-optimal minimum. Figure 5 shows optimal paths of 100 SA runs for LBI.

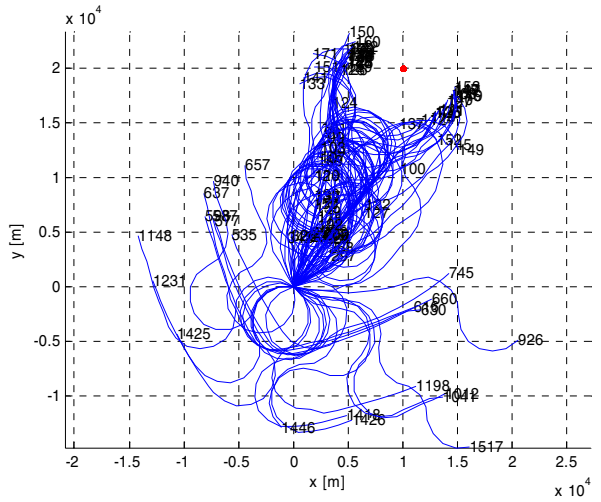

Figure 5 - Optimal paths from simulated annealing The red dot indicates the emitter location.

The tracks start at (0, 0) with the emitter being at (10, 20) km. A track consists of 40 segments of length 1 km (aircraft speed 250 m/s). Constraints are easily incorporated into the SA approach. We used two constraints:

1. The acceleration cannot exceed 20 m/s^2 (2g). This causes the smooth, circular appearance of the tracks.
2. The closest approach distance is 5 km. This accounts for the empty circle around the emitter.

We optimised for minimum error ellipse area. The numbers at the end of the tracks indicate the final minimum area. The tracks ending closest to the emitter have a minimum error ellipse area of about 120-150 m^2. This is similar to findings for bearing measurements [6]: optimal tracks starting "near" the emitter tend towards the emitter while, on the other hand, optimal tracks starting farther away tend to keep manoeuvring at a distance. Optimization finds the right balance between the accuracy gain due to approaching and manoeuvring.
In [6] an example with bearing measurements is used, and the determinant of the FIM (detFIM) is maximized. As a check, we solved this particular optimization problem with SA. The results are in Table 3. *K* is the (constant) aircraft speed times the total flight time divided by the initial range to the emitter. It indicates the degree to which the emitter is within reach. Small *K* lead to manoeuvring at a fixed range, while large *K* lead to track extending towards the emitter. The SA approach provides up to 3 % better results. The SA optimal tracks look very similar to [6].

	***K*= 0.1**	***K*= 0.2**	***K*= 0.4**	***K*= 0.6**
Ref. [6], Table I	1.7202E-4	7.6456E-4	0.0044	0.0190
Simulated annealing	1.7402E-4	7.7487E-4	0.0045	0.0195

Table 3 – detFIM for various optimal trajectories compared.

VI. Software Tools

Two software tools were developed to estimate and compare the performance of location algorithms.

A. Algorithm analyzer

Figure 6 shows the user interface of the algorithm analyzer tool.

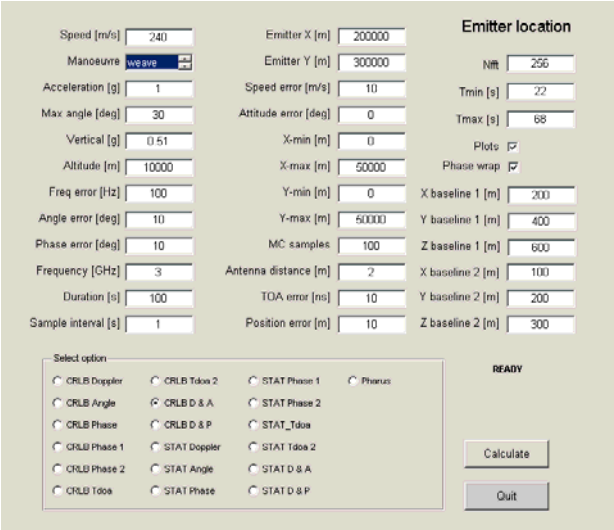

Figure 6 – User interface for the algorithm analyzer.

The algorithm analyzer implements location algorithms based on measurements of:

1. Doppler frequency
2. Bearing

3. Interferometry: 1 platform + 2 antennas / 1 platform + 3 antennas / 2 platforms with 1 antenna each.
4. Time difference of arrival (TDOA).
5. Combinations 1-2 and 1-3.

Typical output is shown in Figure 7: CRLB ellipses on a spatial grid.

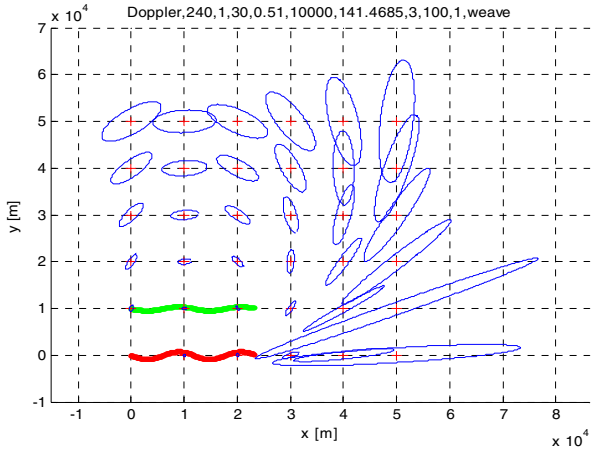

Figure 7 – Typical output of the algorithm analyzer for Doppler location.

The shape of the ellipses depends on the position. For example, the *x*-coordinate estimate of an emitter at (50, 0) km is much worse than its *y*-coordinate estimate. The weaving lines indicate the aircraft track. The lower line is the *xy*-projection, the upper line the *xz*-projection (the average altitude is 10 km).

B. *Dynamic analyzer*

The dynamic analyzer is used to interactively input an aircraft track while the location errors for the Doppler LBI location technique are updated continuously. Figure 8 shows the input (left) and output (right). In this way it is possible to interactively assess the influence of manoeuvring on error ellipse size and orientation, and the rate of accuracy increase.

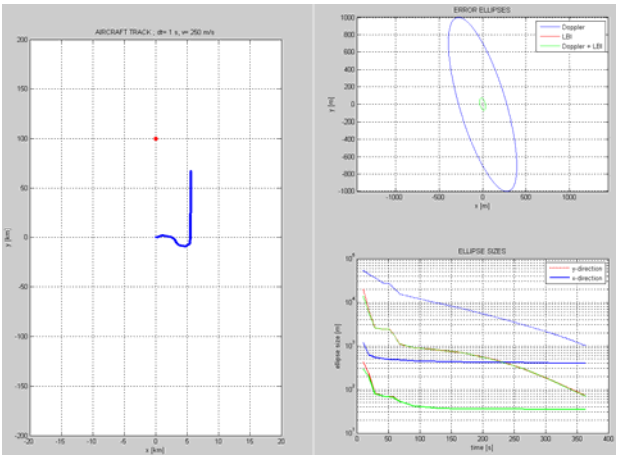

Figure 8 – Output of the interactive dynamic analyzer. Upper right: error ellipses. Lower right: ellipse sizes as a function of time.

VII. APPENDICES

A. *The CRLB*

To arrive at the CRLB we first compute the *N*×4 Jacobian matrix $\mathbf{H} = \left[\mathbf{h}_x \,|\, \mathbf{h}_y \,|\, \mathbf{h}_z \,|\, \mathbf{h}_f\right]$ [1]. Vector $\mathbf{h}_x$ follows from partially differentiating Eq.(1) with respect to x_e:

$$\mathbf{h}_x = \frac{f_0}{cr}\left(v_x - u_x \mathbf{v}(t)\cdot\mathbf{u}(t)\right) \tag{9}$$

with r the radar-emitter distance. $\mathbf{h}_y$ ($\mathbf{h}_z$) is simply obtained by changing x into y (z) in this equation. Differentiation with respect to f_0 gives

$$\mathbf{h}_f = 1 - \frac{\mathbf{v}(t)\cdot\mathbf{u}(t)}{c} \tag{10}$$

We now substitute the N position and frequency measurements to get the N×4 matrix $\mathbf{H}$. The 4×4 element Fisher Information Matrix (FIM) is defined as

$$\mathbf{J} = \mathbf{H}^{\mathrm{T}}\mathbf{C}^{-1}\mathbf{H}, \tag{11}$$

with $\mathbf{C}$ the covariance matrix: the variance σ_f^2 of the RF error noise process $v(t)$ of Eq.(1) times the N×N element unity matrix. The FIM is projected on the *xy*-plane by

$$\mathbf{J}_{\mathrm{proj}} = [\mathbf{P}\,\mathbf{J}^{-1}\mathbf{P}^{\mathrm{T}}]^{-1}, \tag{12}$$

with the projection matrix defined as

$$\mathbf{P} = \begin{pmatrix} 1 & 0 & 0 & 0 \\ 0 & 1 & 0 & 0 \end{pmatrix}. \tag{13}$$

The 2×2 matrix $\mathbf{J}_{\mathrm{proj}}$ defines the CRLB ellipse that contains on average 39 % of the estimated locations. The short and long axis lengths of this ellipse are twice the square roots of the reciprocal eigenvalues of $\mathbf{J}_{\mathrm{proj}}$.
The above can be used to find analytical expressions for the effect of input parameters on the location accuracy. We give an example for the RF error σ_f :

$$\mathbf{J}_{\mathrm{proj}} = [\mathbf{P}\,\mathbf{J}^{-1}\mathbf{P}^{\mathrm{T}}]^{-1} = [\mathbf{P}\,[\mathbf{H}^{\mathrm{T}}\,(\sigma_f^2 \times \mathbf{I})^{-1}\,\mathbf{H}]^{-1}\,\mathbf{P}^{\mathrm{T}}]^{-1} =$$
$$[\mathbf{P}\,[\mathbf{H}^{\mathrm{T}}\,\mathbf{H}]^{-1}\,\mathbf{P}^{\mathrm{T}}]^{-1} / \sigma_f^2 \equiv \mathbf{K} / \sigma_f^2. \tag{14}$$

The eigenvalues of $\mathbf{J}_{\mathrm{proj}}$ are $1/\sigma_f^2$ times the eigenvalues of matrix $\mathbf{K}$, and hence linearly proportional to the RF error.

B. *The CRLB of combined methods*

This appendix is devoted to the problem of deriving the error ellipse of a combined method (e.g., Doppler and LBI) in terms of the ellipses of its constituting methods. We first show the result in Figure 9. It shows ellipses of the separate (dotted, dashed) and combined methods (solid).

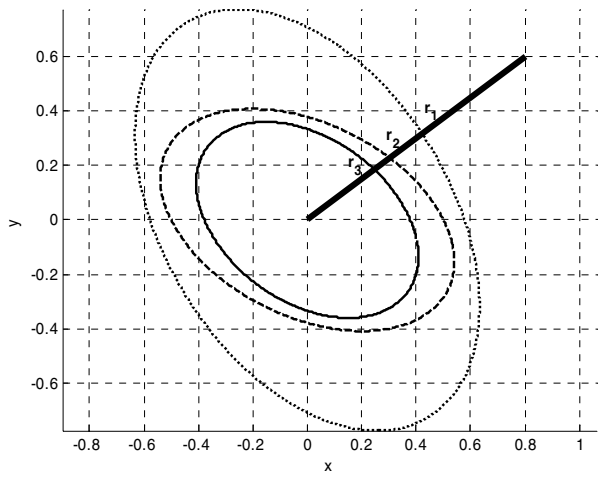

Figure 9 – Error ellipses of separate and combined methods.

The direction of the straight line segment is arbitrary. It crosses the origin. r_1, r_2 and r_3 are the distances between the origin and the intersection of the black line with the dotted, dashed and solid curves, respectively. The following equation now holds:

$$r_3 = \frac{r_1 r_2}{\sqrt{r_1^2 + r_2^2}}. \tag{15}$$

It can be proven to be consistent with the three curves being ellipses. We proceed to sketch a proof of this equation.

An error ellipse follows from a 2D (projected) Fisher information matrix **J**. The ellipse corresponding to a FIM **J** can be drawn by taking a unit vector **x** and plotting the points $\mathbf{J}^{-1/2}\mathbf{x}$ while rotating this vector along the unit circle. From Appendix I follows that the Jacobian matrix of combined methods consist of two stacked sub-matrices, corresponding to the two measurement types. From this and Eq.(11) follows that the combined FIM is the sum of the individual ones. Assume the separate methods have Fisher matrices $\mathbf{J}_1$ and $\mathbf{J}_2$. Than the combined method has Fisher matrix $\mathbf{J}_3 = \mathbf{J}_1 + \mathbf{J}_2$. Because of the way an error ellipse is related to the Fisher matrix we may write

$$\mathbf{J}_1^{-1/2}\mathbf{x} = r_1\mathbf{u} \tag{16}$$

$$\mathbf{J}_2^{-1/2}\mathbf{y} = r_2\mathbf{u} \tag{17}$$

$$\mathbf{J}_3^{-1/2}\mathbf{z} = \left(\mathbf{J}_1 + \mathbf{J}_2\right)^{-1/2}\mathbf{x} = r_3\mathbf{u} \tag{18}$$

The unit vectors **x**, **y** and **z** have generally a different direction. The matrix multiplications at the left hand transform them all in the same direction **u** (also a unit vector)**.** This vector represents the direction of the straight line segment in Figure 9. The top equation is transformed as follows:

$$\mathbf{J}_1^{-1/2}\mathbf{x} = r_1\mathbf{u} \Rightarrow \mathbf{u}^T\mathbf{J}_1\mathbf{u} = \frac{1}{r_1^2}, \tag{19}$$

By transforming Eq.(17) and (18) similarly and combining the results we arrive at Eq.(15). The result can be generalized. If n measurements with 'ellipse sizes' r_i (i= 1...n) are combined to one with r one gets

$$r = \left(\sum_{i=1}^{n}\frac{1}{r_i^2}\right)^{-\frac{1}{2}}. \tag{20}$$

This implies that the combined ellipse is located entirely inside all other ellipses.

VIII. Conclusions

Experiments showed that ground based emitter locations can be estimated from an airborne platform with a relative accuracy of 3%, using Doppler frequency measurements. Some analytical relations for the theoretical accuracy of Doppler and interferometry based methods were given. Combining error ellipses of Doppler and interferometric methods (or any other combination of single location methods) turned out to give an error ellipse which bears a simple relations with the error ellipses of the single methods. Simulated annealing turned out to be a useful technique to find optimal tracks. The results for a particular case were slightly better than those reported elsewhere.

References

[1] M.L. Fowler "Analysis of single-platform passive emitter location with terrain data", *IEEE Tr. on AES*, Vol, 37, No. 2, April 2001, pp.495-507

[2] A. Theil, "Frequency Estimation in ESM Systems for Emitter Location", TNO report, 2008, in preparation

[3] W.H. Press, B.P. Flannery, S.A. Teukolsky and W.T. Vetterling, 'Numerical Recipes – The art of scientific computing', Chapter 10, 1986, Cambridge University Press

[4] N. Levanon, "Interferometry against differential Doppler: performance comparison of two emitter location airborne systems", IEE Proc, Vol. 136, Pt. F, No. 2, April 1989

[5] K. Becker, "An efficient method of passive emitter location", IEEE Tr. on AES, Vol. 28, No. 4, October 1992, pp. 1091-1104

[6] Y. Oshman and P. Davidson, "Optimization of observer trajectories for bearings-only localization", IEEE Tr. AES, Vol. 35, No. 3, July 1999